

## Stress Analysis of a Borehole in Saturated Rocks Under in situ Mechanical, Hydrological and Thermal Interactions

J. C. SHENG,<sup>1,2</sup> J. LIU,<sup>1</sup> W. C. ZHU,<sup>2</sup> D. ELSWORTH,<sup>3</sup>  
 and J. X. LIU<sup>2</sup>

<sup>1</sup>College of Water Conservancy and Hydropower Engineering,  
 Hohai University, Nanjing, Jiangsu, P. R. China

<sup>2</sup>School of Oil & Gas Engineering, The University of Western Australia,  
 Crawley, Western Australia

<sup>3</sup>Energy Institute and Department of Energy and Geo-Environmental  
 Engineering, Pennsylvania State University, University Park,  
 Pennsylvania, USA

**Abstract** *A novel approach is developed to represent coupled thermal-hydraulic-mechanical (THM) behavior of porous systems that incorporates the non-isothermal free and forced convection of a single component fluid in a non-boiling thermoelastic medium. The three-way simultaneous coupling between the THM triplet is currently linear, but no restriction is placed on incorporating material nonlinearities. The coupled PDEs are solved in space by grid-adaptive finite elements. The model is validated against solutions for linear non-isothermal consolidation of a column. We demonstrate the utility of the model by analyzing the behavior of a deep wellbore in a thermoelastic medium circulated by a pressurized, but chilled fluid. Model results illustrate the significant importance of the cross-couplings between individual THM processes for the evaluation of wellbore stability.*

**Keywords** boreholes, coupled thermal-hydraulic-mechanical processes, pore pressure, stress analysis, thermal diffusion, wellbore stability

### Introduction

Coupled thermal-hydrologic-mechanical (THM) processes in porous media are important in a broad range of natural and engineered processes. Important contemporary issues include resource recovery of hydrocarbons, including gas hydrates, and in the safe disposal of wastes, including geologic sequestration of CO<sub>2</sub> and the entombment of radioactive wastes. In all applications, the complexities of process interactions exert a strong control on ultimate behavior—these include linear physical interactions, but also the development of material nonlinearities that irreversibly alter the affected media. This is equally the case in engineering the recovery of hydrocarbons. Oil recovery operations are traditionally divided between primary, secondary, and tertiary stages (Green and Willhite, 1998). All of these recovery processes involve coupled processes. For primary production, accurate prediction of oil production in a pressure-sensitive reservoir requires both mechanical

Address correspondence to J. Liu, School of Oil-Gas Engineering, The University of Western Australia, 35 Stirling Hwy, Crawley, WA. E-mail: Jishan@cyllene.uwa.edu.au

deformation and fluid flow modeling (Minkoff et al., 2003). A set of doubly coupled equations, with a number of coupling relations, are required to quantify the phenomenon. The couplings may be between linear processes, linked in poroelasticity via the principle of effective stress (Biot, 1941), but may also include material nonlinearities such as strain-dependent permeability (Liu et al., 2000). For secondary recovery, a triplet of individual processes (multiphase flow, deformation, and chemical transport) is coupled. A set of triply coupled equations, with a number of coupling relations such as saturation-dependent permeability and flow-dependent chemical transport, are required to quantify the phenomenon. For EOR (tertiary recovery is often termed as enhanced oil recovery, or EOR), a quadruplet of individual processes (multiphase flow, deformation, chemical and thermal transport) is coupled. EOR processes involve the injection of energetic or reactive fluids into a reservoir. A set of quadruply coupled equations with a number of coupled relations is required to quantify the phenomenon. Scientific interest in these coupled processes in geological systems has resulted in a number of research efforts aimed at understanding the coupled thermal, hydrological, chemical, and mechanical (THMC) behaviors of geological systems (Guvanasen and Chan, 2000; Liu and Brady, 2004; Tsang, 1999; Oldenburg et al., 2001; Rutqvist and Tsang, 2003; Rutqvist et al., 2002; Neaupane and Yamabe, 2001; Sheorey et al., 2001).

In this study, we define the coupled THM processes as coupled multiphysics. According to Minkoff et al. (2003), there are three basic algorithms for the simulation of coupled multiphysics: one-way coupling, loose coupling, and full coupling. For one-way coupling, two essentially separate sets of equations are solved independently over the same total time interval. Periodically, output from one simulator is passed as input to the other; however, information is passed in only one direction. An example of successful one-way coupling is available in Fredrich et al., (1998). Several other studies that used a “loose coupling” algorithm to simulate coupled multiphysics phenomena reside somewhere full and one-way coupling (Minkoff et al., 2003; Rutqvist and Tsang, 2003; Tsang, 1999; Oldenburg et al., 2001). In loose coupling, two sets of equations are solved independently (as in one-way coupling), but information is passed at designated time intervals in both directions between the two simulators (fluid flow and geomechanics). To define a fully coupled simulator, a single set of equations (generally a large system of non-linear coupled partial differential equations) incorporating all of the relevant physics must be derived. Full coupling is often the preferred method for simulating multiple types of physics simultaneously since it should theoretically produce the most realistic results. Little progress has so far been reported due to the extreme complexity in simulating multiphysics simultaneously. The primary motivation of this study is to demonstrate our latest success in simulating multiphysics simultaneously by using FEMLAB, the first engineering tool that performs equation-based multiphysics modeling in an interactive environment. With FEMLAB we extend conventional models for one type of physics into multiphysics models that solve coupled physics phenomena, and do so simultaneously. Specifically, we derive a single set of equations incorporating the physics of fluid flow, of solid deformation, and of energy transport in porous media. The cross-couplings among multiple processes are defined by the coupled relations between material properties and independent variables. This approach is detailed in the following.

### **Governing Equations**

In this study, we formulate the coupled equations based on Noorishad and Tsang (1996). Conservation equations for energy, mass, and momentum are derived on the macroscopic

scale (all variables are averaged over the REV of the medium) for a saturated, porous elastic medium.

### Flow Equation

The Eulerian form of the mass balance equation for fluid flow is defined as

$$\frac{\partial(\phi\rho_l)}{\partial t} + \nabla \cdot \phi\rho_l \mathbf{V}_l = Q \quad (1)$$

where  $\phi$  is the porosity in a general continuum,  $\rho_l$  is the liquid density,  $t$  is time (seconds),  $\mathbf{V}_l$  is the velocity vector of the fluid, and  $Q$  is the source term of the fluid. The momentum balance for the fluid flow in porous media under usual assumptions yields the generalized Darcy equation of motion in the Cartesian coordinate system:

$$\mathbf{V}_l = -\frac{\mathbf{k}}{\mu_l} \cdot (\nabla P - \rho_l \mathbf{g}) \quad (2)$$

where  $\mu_l$  is the dynamic fluid viscosity,  $\mathbf{k}$  is the intrinsic permeability tensor in a general continuum,  $P$  is the pore fluid pressure (Pa), and  $\mathbf{g}$  is the vector of gravitational acceleration ( $m/s^2$ ). Substituting Eq. (2) into Eq. (1), and including the deformation of the solid skeleton, the flow Eq. (1) can be rewritten as

$$\frac{\rho_l}{\rho_0} \frac{\partial \varepsilon_v}{\partial t} + \frac{\partial(\phi\rho_l)}{\partial t} - \nabla \cdot \left[ \frac{\rho_l \mathbf{k}}{\mu_l} (\nabla P - \rho_l \mathbf{g}) \right] = Q \quad (3)$$

where  $\rho_0$  is the density of the reference fluid,  $\varepsilon_v$  is the volumetric strain of rock matrix. Using the truncated Taylor series expansion of  $\rho_l$ , the relationship of fluid density with temperature and pressure is defined as

$$\frac{D\rho_l}{Dt} = \rho_0 \beta_T \frac{DT}{Dt} + \rho_0 \beta_P \frac{DP}{Dt} \quad (4)$$

where  $T$  is the temperature,  $\beta_T$  is the coefficient of thermal volume expansion for the liquid,  $\beta_P$  is the compressibility coefficient of the liquid, and  $D/Dt$  represents the substantial or material derivative. Substituting Eq. (4) into Eq. (3) yields the following equation:

$$\frac{\rho_l}{\rho_0} \frac{\partial \varepsilon_v}{\partial t} + \phi \beta_P \frac{\partial P}{\partial t} - \phi \beta_T \frac{\partial T}{\partial t} - \nabla \cdot \left[ \frac{\rho_l \mathbf{k}}{\rho_0 \mu_l} \cdot (\nabla P - \rho_l \mathbf{g}) \right] = Q. \quad (5)$$

Equation (5) is the final form of the governing equation for the moving fluid in a porous thermoelastic medium. The first three terms on the left side of Eq. (5) describe the changes in rock volume due to strain, fluid-pressure, and temperature, respectively. The last term on the left side of Eq. (5) represents the resulting fluid flow driven by the pressure gradient and gravity and moderated by Darcy's law.

### Energy Conservation Equation

The solid skeleton and the fluid coexist within a common control volume, but exhibit different thermodynamic properties, such as specific heat capacity and thermal conductivity. Therefore, equations of energy conservation for the solid skeleton and the fluid

should be defined individually. The energy conservation for the solid skeleton is defined as

$$(1 - \phi)(\rho c_p)_s \frac{\partial T}{\partial t} = (1 - \phi) \nabla \cdot (\mathbf{K}_s \nabla T) + (1 - \phi) q_s. \quad (6)$$

where  $(\rho c_p)_s$  is the thermal capacity,  $\mathbf{K}_s$  is the thermal conductance tensor, and  $q_s$  is the thermal source intensity, all defined for the solid. For the fluid, the corresponding equation for energy conservation is defined as

$$\phi(\rho c_p)_l \frac{\partial T}{\partial t} + (\rho c_p)_l (\mathbf{V}_l \cdot \nabla) T = \phi \nabla \cdot (\mathbf{K}_l \nabla T) + \phi q_l \quad (7)$$

where  $(\rho c_p)_l$ ,  $\mathbf{K}_l$ , and  $q_l$  are as defined previously, but with the subscripted  $l$  representing the liquid (fluid) component. In a single phase flow system, using the assumption of thermal equilibrium between the solid and the fluid, and combining Eq. (6) with Eq. (7), yields the following uniform equation of energy conservation:

$$(\rho c_p)_t \frac{\partial T}{\partial t} + (\rho c_p)_t (\mathbf{V}_l \cdot \nabla) T = \nabla \cdot (\mathbf{K}_t \cdot \nabla T) + q_t \quad (8)$$

where  $(\rho c_p)_t$  and  $\mathbf{K}_t$  are the specific heat capacity and thermal conductivity of the fluid-filled medium, defined as  $(\rho c_p)_t = \phi(\rho c_p)_l + (1 - \phi)(\rho c_p)_s$ ,  $\mathbf{K}_t = \phi \mathbf{K}_l + (1 - \phi) \mathbf{K}_s$ , respectively.  $q_t$  is the source term applied to the fluid-filled medium, defined as  $q_t = \phi q_l + (1 - \phi) q_s$ , but generally defined only as an aggregate input to a control volume.  $c_{pl}$  and  $c_{ps}$  are the fluid and solid specific heat constants at constant volume. For an isotropic system with respect to the flow of both heat and fluid, Eq. (8) with the energy of deformation also accommodated can be written as (Noorishad and Tsang, 1996):

$$\zeta \frac{\partial T}{\partial t} + (1 - \phi) T_0 \gamma \frac{\partial \varepsilon_v}{\partial t} + (\mathbf{V}_l \cdot \nabla) T = \alpha_t \nabla^2 T + \frac{q_t}{(\rho c_p)_f} \quad (9)$$

where,  $\zeta = (\rho c_p)_t / (\rho c_p)_l$ ,  $\alpha_t = k_t / (\rho c_p)_l$ , and  $k_t$  is the thermal conductivity coefficient of the fluid-filled medium, and  $T_0$  is the absolute temperature in the stress-free state,  $\gamma = (2\mu + 3\lambda)\beta$ ,  $\lambda$  and  $\mu$  are the Lamé constants and  $\beta$  is the linear isotropic coefficient of solid thermal expansion. The deformation energy conversion term,  $T_0 \beta \partial \varepsilon_v / \partial t$ , is not a major contributing term to the energy balance, and can be dropped from the equation if desired.

### **Mechanical Equilibrium Equation**

The constitutive equation defines the relation between the total bulk stress components,  $\sigma_{ij}$ , strain components,  $\varepsilon_{ij}$ , fluid pressure  $P$ , and the thermal stresses,  $\sigma_{Tij}$ .

For the mechanically isotropic case, the stress-strain law is defined as follows:

$$\sigma_{ij} = D_{ijkl} (\varepsilon_{kl} - \varepsilon_{Tkl}) - \alpha \delta_{ij} P, \quad i, j = 1, 2, 3 \quad (10)$$

where  $D_{ijkl}$  is the elasticity tensor,  $\alpha$  is the Biot coefficient partitioning fluid pressure and total stress to effective stress, and  $\delta_{ij}$  is the Kronecker delta defined as 1 for  $i = j$  and 0 for  $i \neq j$ . Under condition of thermal isotropy, Eq. (10) can be written as

$$\sigma_{ij} = D_{ijkl} \varepsilon_{kl} - \gamma \delta_{ij} T - \alpha \delta_{ij} P. \quad (11)$$

The dependent variables ( $\varepsilon$ ,  $P$ , and  $T$ ) in Eq. (11) are all incremental and represent deviation from the zero (stress-free) state. Using compact notation, the equilibrium equation is defined as

$$-\sigma_{ij,j} = F_i. \quad (12)$$

where  $\sigma_{ij}$  is the stress tensor, and  $F_i$  is the component of the body force. Substituting Eq. (11) and the strain-displacement relations into the equation of static equilibrium (Eq. (12)) yields Navier's equation of equilibrium expressed in terms of displacements. Under static conditions, and including thermal effects, Navier's equation is defined as

$$GU_{i,jj} + \frac{G}{1-2\nu}U_{j,ji} - \alpha p_{,i} - \gamma T_{,i} + F_i = 0 \quad (13)$$

where  $U_i$  is the displacement of the solid skeleton, and  $G$  is the shear modulus.

### Validation Example

Equations (5), (9), and (13) with essential boundary and initial conditions define the fully coupled THM system in a saturated elastic medium. This complete set of coupled equations is implemented into, and solved, by using FEMLAB. FEMLAB is a powerful multiphysics simulator with a broad range of applicability in science and engineering. Its main strength is the ability to simulate coupled processes that are modelled with partial differential equations (PDEs). In the following, we validate our FEMLAB-based model by comparison with known solutions.

Noorishad and Tsang (1996) used a coupled finite element code to analyse the thermoelastic consolidation of a sand column. The data used in this problem are given in Table 1. We use our FEMLAB-based model to simulate both the isothermal consolidation and the thermoelastic consolidation. Comparisons between predictions by the two codes are shown in Figure 1. For the case of isothermal consolidation, our results compare quite well with Biot's analytic solution (Biot, 1941). For thermoelastic consolidation, our results also compare well with Noorishad's and Tsang's (1996) solution.

### Application Example

Wellbore stability is one of many serious problems in the oil and gas industry. In most cases, the instability of a wellbore is a coupled THM phenomenon. Thermal diffusion inside the drilled formation induces additional pore pressure, changes rock stress, and consequently affects wellbore stability (Wang et al., 2003). This problem has previously been solved by one-way coupling or "loose coupling" using an algorithm that is partially decoupled (Chen et al., 2003). In the following, we apply our FEMLAB-based model to solve this problem as a fully coupled THM system.

### Model Description

The problem domain and boundary conditions are illustrated in Figure 2. A wellbore of 0.1 m radius is embedded within a square problem of  $2 \times 2$  m. Constant stresses are applied in both the vertical ( $Sh_{min} = 20$  MPa) and the horizontal ( $Sh_{max} = 30$  MPa) directions. The temperature and fluid pressure at the wellbore wall are assumed to be

**Table 1**  
Rock properties used for the consolidation cases and the application example

Parameters	Validation example	Application example
Rock density, $\rho_s$ ( $\text{kgm}^{-3}$ )	NA	2,600
Young's modulus, $E$ (MPa)	$6.0 \times 10^{-3}$	5,000
Rock thermal conductivity, $\mathbf{K}_r$ ( $\text{kJm}^{-1}\text{s}^{-1}\text{C}^{-1}$ )	$8.36 \times 10^{-1}$	$3.08 \times 10^{-3}$
Rock thermal expansion coefficient, $\beta$ ( $^{\circ}\text{C}^{-1}$ )	$3.0 \times 10^{-7}$	$1.0 \times 10^{-5}$
Rock specific heat, $c_{ps}$ ( $\text{kcalkg}^{-1}\text{C}^{-1}$ )	NA	0.20
Specific heat, $(\rho c)_t$ ( $\text{kJm}^{-3}\text{C}^{-1}$ )	167.0	
Matrix porosity, $\phi$	0.2	0.2
Matrix permeability, $\mathbf{k}$ ( $\text{m}^2$ )	$4.0 \times 10^{-6}$	$5.0 \times 10^{-13}$
Biot's coefficient, $\alpha$	1.0	1.0
Poisson's ratio, $\nu$	0.4	0.25
Fluid density, $\rho_l$ ( $\text{kgm}^{-3}$ )	NA	1,000.0
Fluid compressibility, $\beta_p$ ( $\text{GPa}^{-1}$ )	NA	0.513
Dynamic viscosity at 20°C, $\eta$ ( $\text{Nsm}^{-2}$ )	NA	$10^{-3}$
Fluid thermal expansion coefficient, $\beta_T$ ( $^{\circ}\text{C}^{-1}$ )	NA	$3.17 \times 10^{-4}$
Fluid specific heat, $c_{pl}$ ( $\text{kcalkg}^{-1}\text{C}^{-1}$ )	NA	1.0

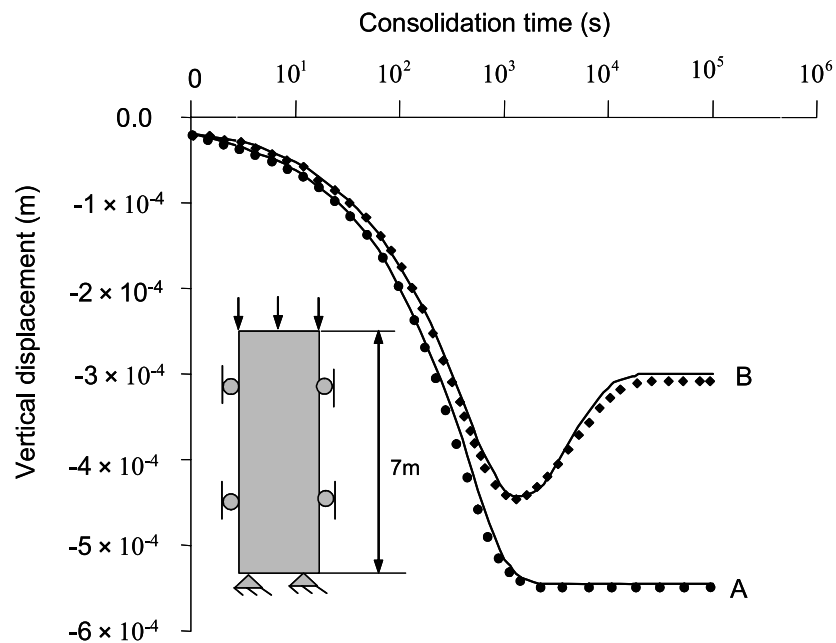


**Figure 1.** Comparisons of FEMLAB simulation results with the known solutions, where simulation data are represented by the symbols while the known solutions are represented by the solid lines. A: Comparison with Biot's (1941) analytical solution for the consolidated history of a sand column without thermal effects. B: Comparison with results of Noorishad and Tsang (1996) with thermal effects.

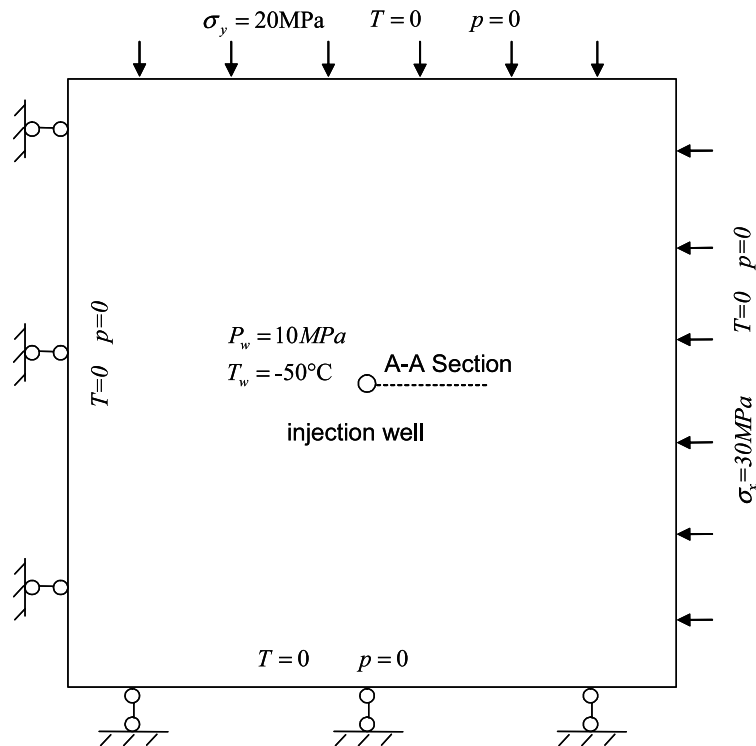


**Figure 2.** Problem definition. Constant compressive pressures, temperatures, and fluid pressures are applied on outside and inside boundary conditions.

equal to the temperature and the pressure of the drilling fluid in the annulus. These are set as temperature and pressure differentials between the formation and the drilling fluid as  $-50^{\circ}\text{C}$  and 10 MPa, respectively. Null temperatures and pore pressures are defined within the rock formation. The properties of the rock and fluid are given in Table 1.

### Model Cases

Four different cases are simulated to illustrate the relative importance of cross couplings. These four cases are:

- Case 1: Mechanical process only, i.e.,  $\Delta p = 0$  MPa,  $\Delta T = 0^{\circ}\text{C}$ , where  $\Delta p = p_w - p_0$  and  $\Delta T = T_w - T_0$ .
- Case 2: Coupled mechanical-thermal processes, i.e.,  $\Delta p = 0$  MPa,  $\Delta T = -50^{\circ}\text{C}$ .
- Case 3: Coupled mechanical-thermal-hydrological processes, i.e.,  $\Delta p = 10$  MPa,  $\Delta T = -50^{\circ}\text{C}$ .
- Case 4: Uncoupled mechanical-thermal-hydrological processes, i.e.,  $\Delta p = 10$  MPa,  $\Delta T = -50^{\circ}\text{C}$ .

There are no coupled terms of  $\rho_l/\rho_0\partial\varepsilon_v/\partial t$  and in Eq. (5), and no coupled terms of  $(1-\phi)T_0\gamma\partial\varepsilon_v/\partial t$  and  $(\mathbf{V}_l \cdot \nabla)T$  in Eq. (9). In this example, rock permeability is very high ( $5.0 \times 10^{-13}$  m<sup>2</sup>), so only the coupled term of convective heat transport  $(\mathbf{V}_l \cdot \nabla)T$  has significant effect on multiphysics process.

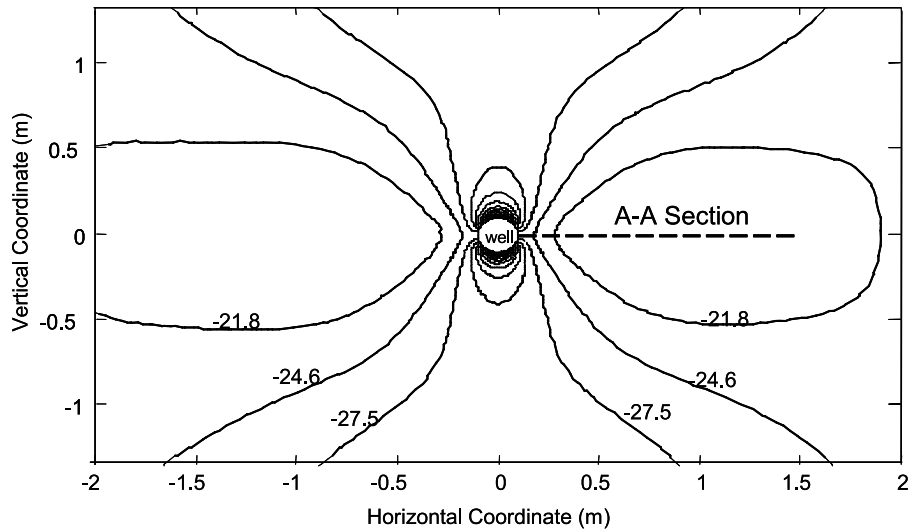


**Figure 3.** Contours of tangential stress (MPa) at time = 86400s for the case of fully coupled mechanical-thermal-hydrological processes.

#### Comparison of Tangential Stresses

Model results of the tangential stress,  $\sigma_{\theta\theta}$  for these four cases are shown in Figures 3 to 5. Figure 3 shows contours of tangential stress at time of 86400s for case 3. From Figure 3, we can see that the stress concentration occurs on the wellbore wall at the directions of  $\theta = \pm 90^\circ$ . The maximum magnitude of the compressive tangential stress

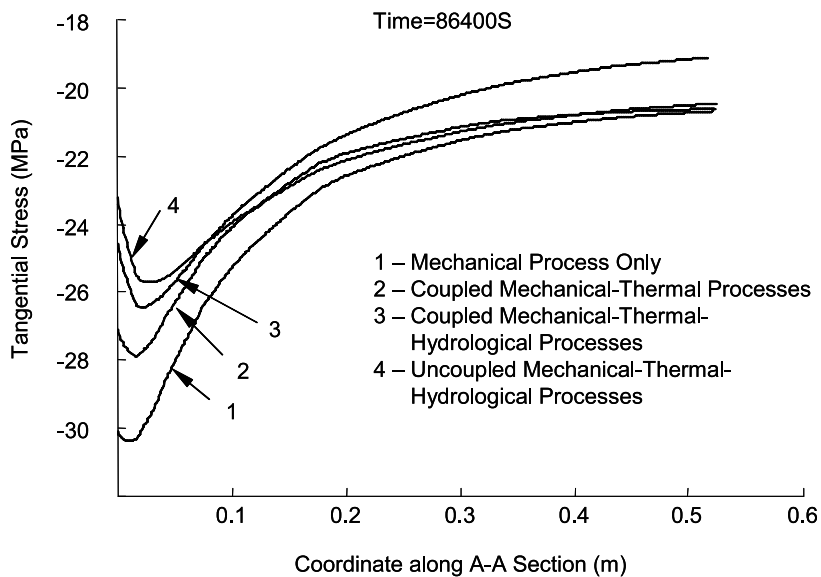


**Figure 4.** Variations of tangential stress (MPa) along the A-A section at time = 86400s for different cases.

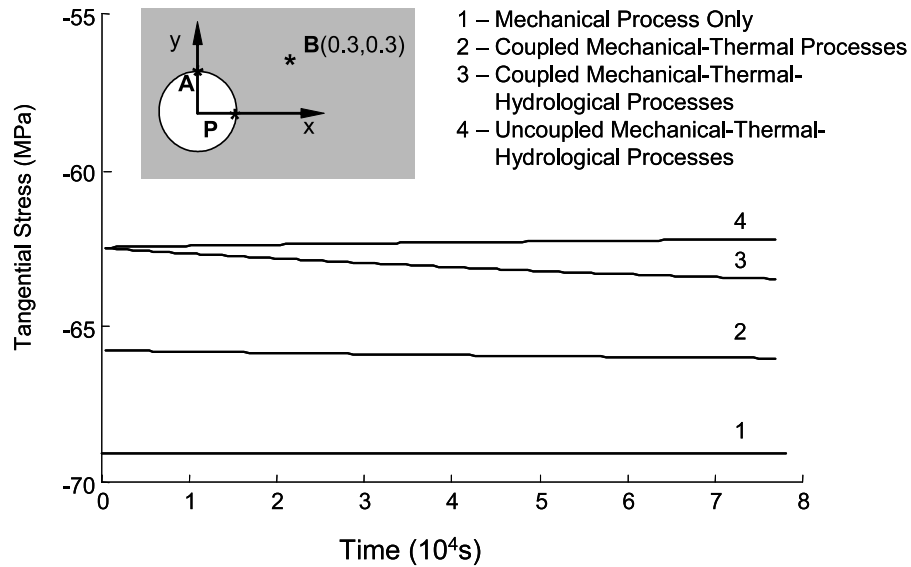


Figure 5. Variations of tangential stress with time at Point A for different cases.

reaches about 65 MPa on the wellbore wall at the directions of  $\theta = \pm 90^\circ$ , and the minimum tangential stress on the wellbore wall is about 25 MPa, which occurs at the directions of  $\theta = 0^\circ$  and  $180^\circ$ . Figure 4 shows variations of the tangential stress with radius at the time of 86400s for four cases. Model results illustrate that the magnitude of the compressive tangential stress,  $\sigma_{\theta\theta}$ , in the vicinity of the wellbore decreases with the temperature and the pore pressure, as shown in Figure 4 for Cases 1 through 3. This is induced by cooling shrink and the effect of pore pressure as cooling process and fluid transport inside the rock formation. Through comparing the magnitudes of  $\sigma_{\theta\theta}$  in Figure 4 for Case 3 and Case 4, we can conclude that there is a big difference for tangential stress between coupled T-M-H system and uncoupled T-M-H system. On the wellbore wall, the magnitude of compressive tangential stress for the coupled T-H-M system is 1.35 MPa larger than that for the uncoupled system (see Table 2). On the contrary, the magnitude of the compressive tangential stress for the coupled T-H-M system is smaller than that for the uncoupled system inside rock formation. This difference is mainly induced by heat transport process. The heat transport process in the coupled T-H-M system is dramatically faster than that in the uncoupled system because of the convective heat transport. Variations of the tangential stress with time for different cases are shown in Figure 5 for the point of A. From Figure 5, we can clearly see the effects of cooling processes and fluid diffusion on the tangential stress. It can be also seen that the variation

**Table 2**  
Comparison of stresses at  $t = 86400$ s of four cases

	Case 1, MPa	Case 2, MPa	Case 3, MPa	Case 4, MPa
$\sigma_{\theta\theta}$ at point P	-30.65	-27.65	-25.14	-23.79
$\sigma_{rr}$ at point B	-23.61	-22.81	-24.66	-24.98

of  $\sigma_{\theta\theta}$  at Point A (0, 0.1) on the wellbore wall in the coupled T-H-M system (case 3) increases with time while the variation of  $\sigma_{\theta\theta}$  with time in the uncoupled system (case 4) decreases slowly.

### Comparison of Radial Stresses

Model results of the radial stress,  $\sigma_{\theta\theta}$  for these four cases are shown in Figures 6 to 8. Figure 6 shows contours of radial stress at the time of 86400s for case 3. The magnitude of the radial stress is equal to pore pressure. We also note that the gradient of the radial stress along directions of  $\theta = 0$  and  $\pi$  is larger than those of  $\theta = \pm\pi/2$ . Figure 7 shows variations of the tangential stress with radius at the time of 86400s for four cases. The comparison of the compressive radial stress,  $\sigma_{rr}$ , at point B of the wellbore wall is given in Table 2 for  $t = 86400$ s. Model results illustrate that the magnitude of the compressive radial stress,  $\sigma_{rr}$ , in the vicinity of the wellbore wall at the direction  $\theta = 0^\circ$  decreases when the temperature at the wellbore (comparing the results of Case 1 with Case 2) decreases, and increases with the pore pressure (comparing the results of Case 2 with Case 3). Through comparing the magnitudes of  $\sigma_{rr}$  in Figure 7 in the coupled system (Case 3) and the uncoupled system (Case 4), we conclude that the magnitude of the compressive radial stress in the coupled T-M-H system is smaller than that in the uncoupled T-M-H system. The difference of  $\sigma_{rr}$  between Case 3 and Case 4 increases as the distance to the wellbore wall increases. Variations of the radial stress with time are shown in Figure 8 for point B (0.3, 0.3) in the vicinity of wellbore wall. The significant difference in  $\sigma_{rr}$  exists between Case 3 and Case 4. The radial stress at point B decreases

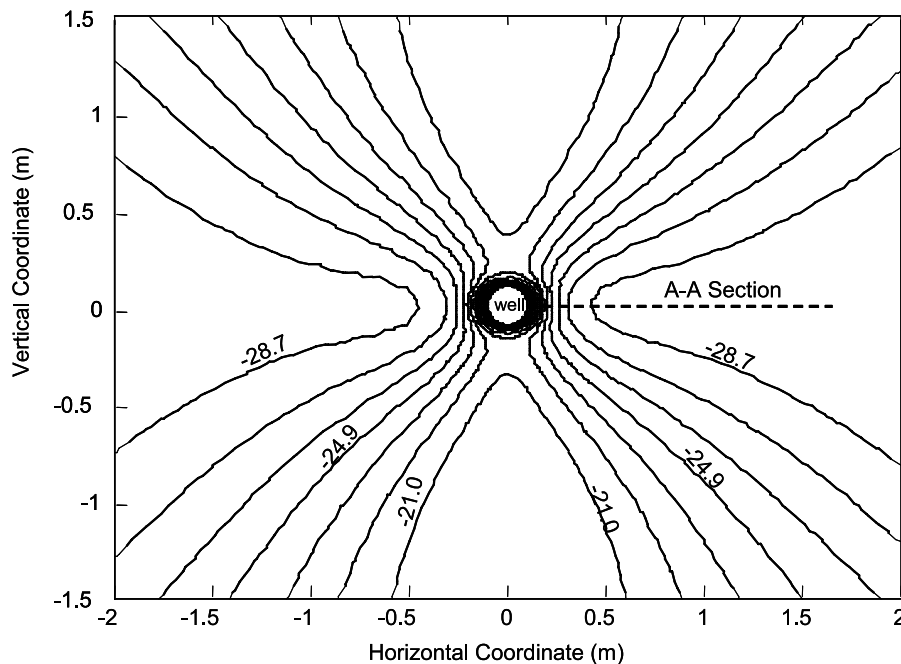


**Figure 6.** Contours of radial stress (MPa) at time = 86400s for the case of fully coupled mechanical-thermal-hydrological processes.

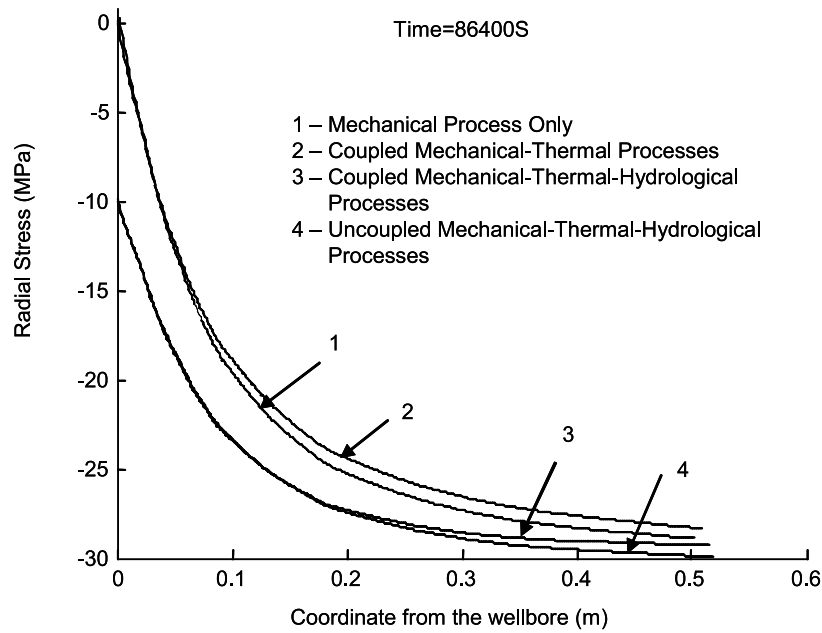


**Figure 7.** Variations of radial stress (MPa) along the A-A section at time = 86400s for different cases.

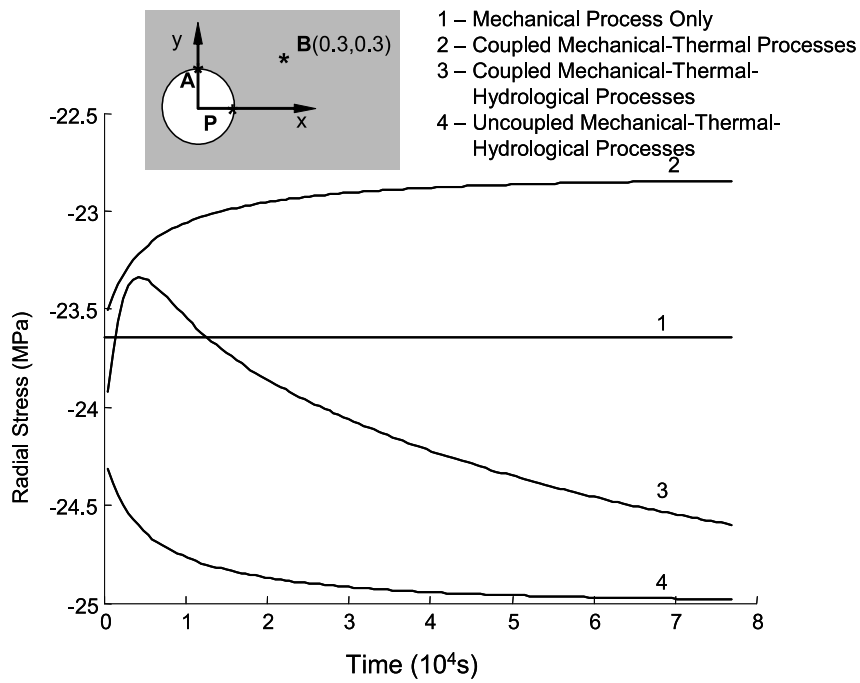


**Figure 8.** Variations of radial stress with time at Point B for different cases.

with time for the first 5000s, and then increases with time thereafter. This is because temperature transfers faster and its effect on the radius stress is larger than that of pore pressure during the first 5000s, then the effect of pore pressure dominates.

## Conclusions

In this study, a novel approach has been developed to solve the fully coupled hydrological, thermal, and mechanical system in rocks. The uniqueness of this approach is that we solve the coupled system in an interactive environment. This allows us to visualize the multi-physical interactions without any difficulties. The validity of this approach has been demonstrated through successful validation against available analytical and numerical solutions for the one-dimensional isothermal and non-isothermal consolidation problem and the simulation of coupled hydrological, mechanical, and thermal processes that affect wellbore stability. Through these simulation examples, we summarize the advantages of this novel approach as follows:

The full coupling of multi-physical processes in rocks was achieved in an interactive environment. In this approach, we extend conventional models for the coupled mechanics of solid deformation, fluid flow, and heat transfer into a single multi-physics model that solves the coupled multiphysics, and does so simultaneously.

The interwoven constitutive relations among different physical systems are straightforwardly implemented into this single multi-physics model because of the interactive environment. In this approach, the complex couplings of the various constitutive relations are algorithmically translated into the coefficient matrices via the high-level symbolic language of FEMLAB. This allows us to introduce any new constitutive relations easily.

Model results are readily presented and visualized both as stills and as movies. By solving this single multi-physics model, we transform the complex science behind coupled phenomena that may be readily incorporated into realistic models of physical processes.

## Acknowledgments

This work is supported by ARC-DP0209425, ARC-LX0242407 and ARC-DP0342446, and also supported by the National Natural Science Foundation of China (50779012) and open fund of the national laboratory of geological hazard prevention and geological environment protection, Chengdu University of Technology (GZ2005-02). These supports are gratefully acknowledged.

## References

- Biot, M. A. 1941. General theory of three-dimensional consolidation. *J. Appl. Phys.* 12:144–164.
- Chen, G. Z., Chenevert, M. E., Sharma, M. M., and Yu, M. J. 2003. A study of wellbore stability in shales including poroelastic, chemical effects. *J. Petrol. Sci. Eng.* 38:167–176.
- Fredrich, J., Detrick, G., Arguello, J., and de Rouffignac, E. 1998. Reservoir compaction, surface subsidence, and casing damage: A geomechanics approach to mitigation and reservoir management. *Proceedings of SPE/ISRM EUROCK*. No. 47284.
- Green, D. W., and Willhite, G. P. 1998. *Enhanced Oil Recovery*. SPE Textbook Series Vol. 6, Society of Petroleum Engineers, Richardson, TX.
- Guvanasen, V., and Chan, T. 2000. A three-dimensional numerical model for thermohydrromechanical deformation with hysteresis in a fractured rock mass. *Intl. J. Rock Mech. Mining Sci.* 37:89–106.

- Liu, J., Elsworth, D., Brady, B. H., and Mulhaus, H. 2000. Strain-dependent fluid flow defined through rock mass classification schemes. *R. Mech. and R. Eng.* 33:75–92.
- Liu, J., and Brady, B. H. 2004. Simulations of a coupled hydro-chemo-mechanical system in rocks. *Geotech. Geolog. Eng.* 22:121–133.
- Minkoff, S. E., Stone, C. M., Bryant, S., Peszynska, M., and Wheeler, M. F. 2003. Coupled fluid flow and geomechanical deformation modelling. *J. Petrol. Sci. Eng.* 38:37–56.
- Neaupane, K. M., and Yamabe, T. 2001. A fully coupled thermo-hydro-mechanical nonlinear model for a frozen medium. *Comp. Geotech.* 22:613–637.
- Noorishad, J., and Tsang, C.-F. 1996. Coupled thermohydroelasticity phenomena in variably saturated fractured porous rocks—formulation and numerical solution. In: *Coupled Thermo-Hydro-Mechanical Processes of Fractured Media*, Stephansson, O., Jing, L., and Tsang, C. F. (Eds.). Amsterdam: Elsevier Science Publishers, pp. 93–134.
- Oldenburg, C. M., Pruess, K., and Bensen, S. M. 2001. Process modeling of CO<sub>2</sub> injection into natural gas reservoirs for carbon sequestration and enhanced gas recovery. *Energy and Fuels* 15:293–298.
- Rutqvist, J., Tsang, C. F. 2003. Analysis of thermal-hydrologic-mechanical behavior near an emplacement drift at Yucca Mountain. *J. Contaminant Hydrol.* 62–63:637–652.
- Rutqvist, J., Wu, Y. S., Tsang, C. F., and Bodvarsson, G. 2002. A modelling approach of coupled multiphase fluid flow, heat transfer, and deformation in fractured porous rock. *Int. J. Rock Mech. & Min. Sci.* 39:429–442.
- Sheorey, T., Muralidhar, K., and Mukherjee, P. P. 2001. Numerical experiments in the simulation of enhanced oil recovery from a porous formation. *Int. J. Therm. Sci.* 40:981–997.
- Tsang, C. F. 1999. Linking thermal, hydrological, and mechanical processes in fractured rocks. *Annu. Rev. Earth Planet. Sci.* 27:359–384.
- Wang, Y. L., and Dusseault, M. B. 2003. A coupled conductive-convective thermal-poroelastic solution and implications for wellbore stability. *J. Petrol. Sci. Eng.* 38:187–198.